IMPACT DYNAMICS OF HIGH SPEED ROTORS IN RETAINER BEARINGS AND MEASUREMENT CONCEPTS

M. Fumagalli, P. Varadi, G. Schweitzer
International Center for Magnetic Bearings, ETH, Switzerland

ABSTRACT
This paper presents results on the impact dynamics of a high speed rigid rotor in a simple rigid retainer bearing with small clearance. The contact between the rotor and the bearing is modelled with the Coulomb-friction law and the coefficient of restitution.
To measure the contact force and the contact time during the impact, we have developed a force sensing device based on Hertz Impact Theory.
Analysis shows that a small air-gap is an important parameter, which influences to the whirling motion of the rotor around the bearing.

INTRODUCTION

A retainer bearing protects the active magnetic bearing (AMB) assembly from direct contact with the rotor. It prevents damage during the maintenance, and destruction of the system after a possible AMB failure [1].
The retainer bearings are thus a central safety component of a AMB-system and it is essential to understand their performance. A failure of the retainer bearing itself jeopardises the full potential of this technology.Various studies have been performed to understand the influence of parameters on the dynamics. Kirk [2] demonstrated that there is an optimum damping to minimize the rotor's response and the contact force. Schmied [3] showed numerically the influence of damping on the whirling motion of the rotor. In our previous work [4] we examined the parameter effects for a rotor sliding in a simple cylindrical mode of motion. For a more general model, however, we showed that a purely cylindrical or conical motions do not exist.
In this paper we investigate the impact dynamics for a horizontal rotor. The contribution of parameters such as friction, air-gap and damping to the rotor whirl is examined as well. Additionally, measurement concepts are proposed. To measure the contact force and prove the safety of the system we have been building an AMB experimental platform, where different kinds of motions, forces and energy losses may be measured and analysed.

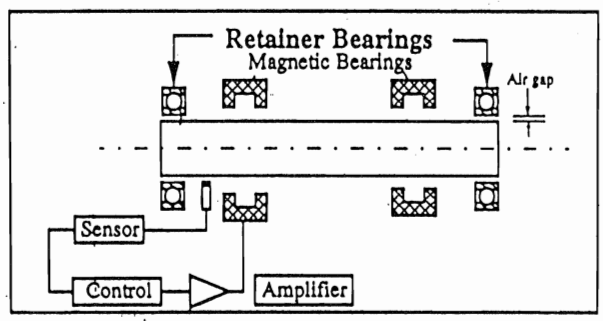

FIGURE 1: Magnetic Bearings Assembly

PHASES OF MOTION

The touchdown process can be characterised by four distinct phases of motion [5]. These are: free-fall, impact, sliding and eventually rolling.
Like in our previous paper [4], we built a planar model on the assumptions that a cylindrical motion exists and is stable.
The motion of the rotor's center of mass is defined in polar coordinates (Figure 2). The angular coordinate is θ and the radial coordinate is ρ. The respective time derivatives are $\dot{\theta}$, $\dot{\rho}$.
The rotor (radius r, mass m) and the bearing (radius R) are considered to be rigid. Sliding motion of the rotor is governed by Coulomb friction μ. The air gap is $\rho_0 = (R - r)$.

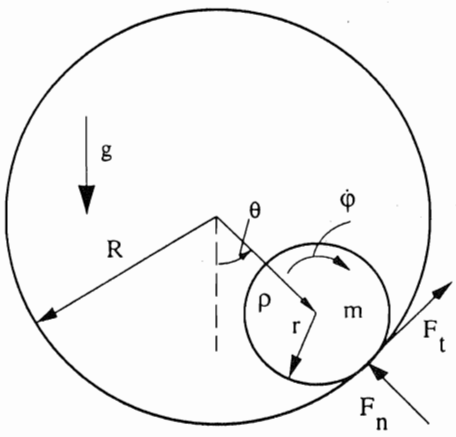

FIGURE 2: Geometry of the Contact Model

The free fall phase of the rotor is represented by the following equations of motion:

$$\ddot{\theta}\rho = -2\dot{\rho}\dot{\theta} - g\sin\theta \qquad (1)$$

$$\ddot{\rho} = \rho\dot{\theta}^2 + g\cos\theta \qquad (2)$$

An impact occurs for $\rho(t) = \rho_0$. Under the assumption that the rotor does not change its position during this impact, the integrated equations of motion are:

$$m(\dot{\rho}^+ - \dot{\rho}^-) = -\int_0^{T_c} F_n \, dt \qquad (3)$$

in the normal direction, and

$$m\rho_0(\dot{\theta}^+ - \dot{\theta}^-) = \int_0^{T_c} F_t \, dt \qquad (4)$$

in the tangential direction.
The superscripted plus and minus signs represent the quantities before and after the impact. The impact time T_c is expected to be very small.
The friction and the normal force are related by

$$F_t = \mu F_n \qquad (5)$$

for the sliding rotor.
The coefficient of restitution $\varepsilon \geq 0$ relates the radial velocities:

$$\dot{\rho}^+ = -\varepsilon \dot{\rho}^- \qquad (6)$$

It describes the grade of contact plasticity: $\varepsilon = 1$ implies elastic impact and $\varepsilon < 1$ inelastic impact.
Together with equations 3 and 4 we obtain:

$$\dot{\theta}^+ = \dot{\theta}^- + \frac{\mu(1+\varepsilon)}{\rho_0}\dot{\rho}^- \qquad (7)$$

Equations 6 and 7 are the kinematic impact relations for both degrees of freedom.

When the rotor makes permanent contact with the bearing, its motion will be cylindrical, thus $\rho = \rho_0$, $\dot{\rho} = 0$. The equations of motion for this phase and their analysis have been proposed in [4]. Figure 3 shows the numerically integrated phase trajectories in the $(\theta, \dot{\theta})$ phase plane.

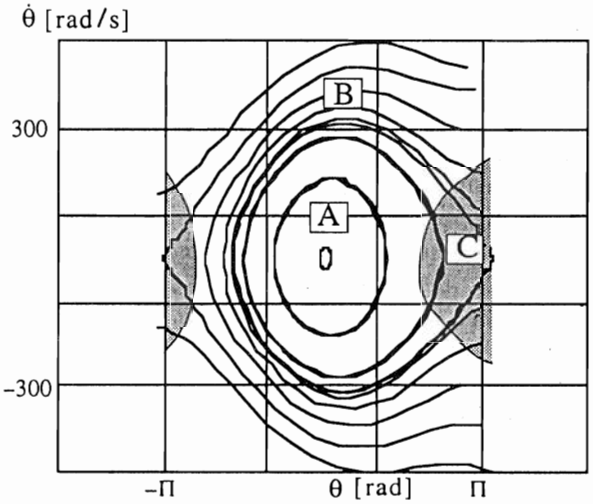

FIGURE 3: Cylindrical Motion in the Phase Plane

They show some distinct features. There are periodic motions inside region A, approaching the oscillatory behaviour of a pendulum. Inside region B, the rotor whirls around the bearing.
When it crosses into the region C - in which the normal contact force would become negative - the contact with the bearing is lost and a free fall takes place, again followed by series of impacts.

NUMERICAL SIMULATION

Complete rotor crash after AMB failure have been simulated for different initial positions (θ, ρ).

In Figure 4a, the rotor first undergoes a transient series of impacts, which looks chaotic. After this, it makes permanent contact with the bearing and goes into cylindrical whirl.

Figure 4b shows a different scenario. After the impact series, the rotor stays at the bottom of the bearing, oscillating back and forth like a pendulum.

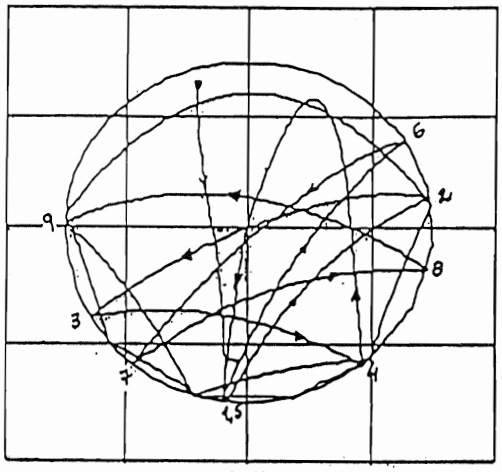

Figure a. Cylindrical Motion

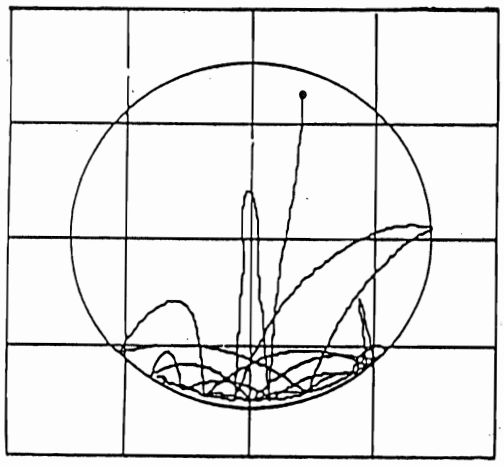

Figure b. Oscillatory Motion

FIGURE 4: Motions after a Failure

INFLUENCE OF PARAMETERS

As we have seen in Figure 3, high angular velocities $\dot{\theta}$ are needed to cause the rotor whirling around the bearing.

During an impact series, a substantial increase of $\dot{\theta}$ is obtained due to the coefficient $\kappa = \mu(1+\varepsilon)/\rho_0$ (see equation 7).

As an example, for $\varepsilon = 0.8, \mu = 0.1$ and $\rho_0 = 0.3\text{mm}$, we obtain $\kappa = 600\text{m}^{-1}$. This value has to be compared with the initial velocities $(\dot{\theta}^-, \dot{\rho}^-)$ in equation 7, which however are generally unpredictable. To get the right order of magnitude, let's assume that the rotor falls from a height ρ_0.

In this case, the velocities at the first contact become $\dot{\theta}^- = 0$, and $\dot{\rho}^- = \sqrt{2g\rho_0} \cong 0.1$ m/s, and therefore $\dot{\theta}^+ = 60$ rad/s.

The next impact would increase $\dot{\theta}$ by another 48 rad/s (see also equation 6). Further analysis shows that the angular speed necessary for whirl may not be reached (350 rad/s in Figure 3).

This example shows that we must keep κ as small as possible in order to bring the rotor into the pendulum-like behaviour rather than the whirl. So, ρ_0 should be large.

Remember that the magnetic forces are inversely proportional to the air-gaps, and therefore large air-gaps are undesirable in magnetic bearings and therefore, for the final design of retainer bearings with small air-gaps, small friction and high damping (small ε) should be considered.

Experimental Concepts

We have built a small rotor, to have a rotor with a high bending stiffness.

The design features have the following characteristics:

- Maximum speed of the rotor: 30' 000 rpm
- Length of rotor: 326mm
- Rotor weight: 3.42 kg
- Maximum rotor diameter: 48mm
- Motor: 300 W

The maximal rotational speed of the rotor (500Hz) is less than the frequency of the first elastical mode (1520Hz). The first mode shape of the shaft is shown in Figure 5.

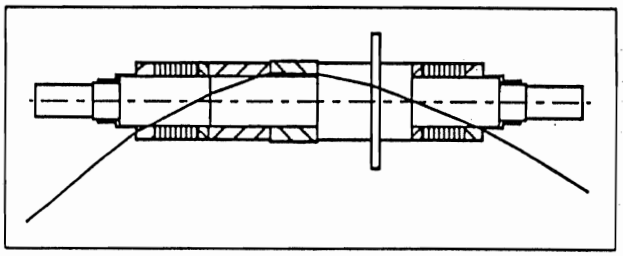

FIGURE 5: First Elastic Mode of the Rotor

Given the maximal rotational speed we can determine the necessary strength of the material that has to be used for the rotor, following design procedures given in [6].

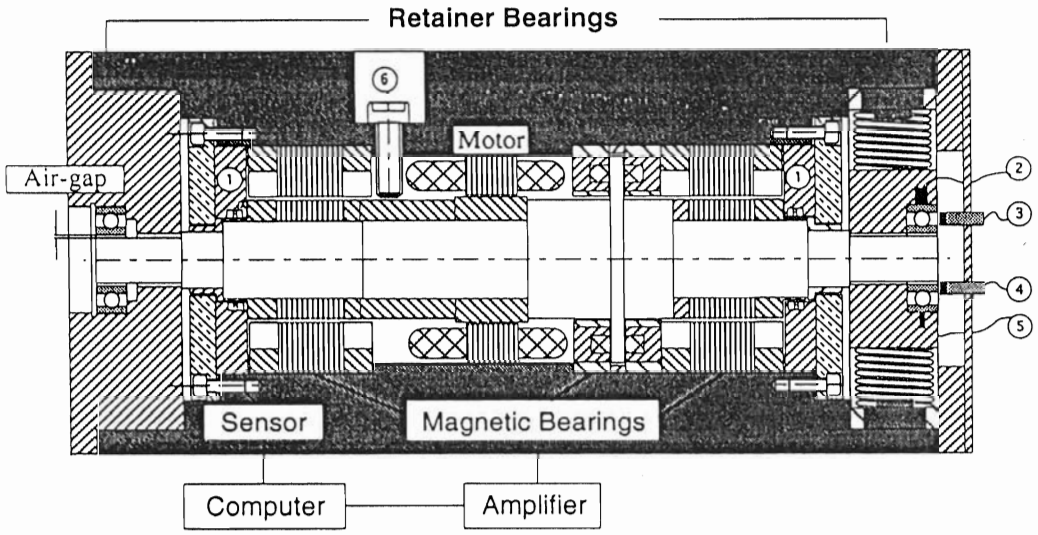

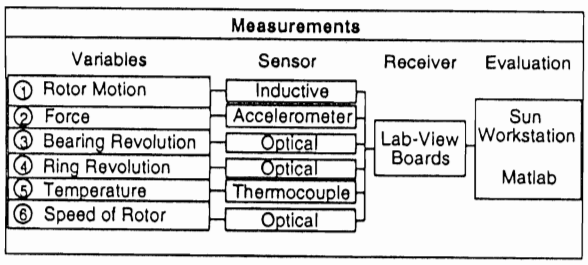

FIGURE 6: Experimental Set up

Furthermore, we must ensure a high level of safety. To achieve this, our experimental set up has a high clearance between the bearings and the rotor. This air-gap is 0.75mm, the air-gap between the rotor and the motor is 0.80mm. The retainer bearing will be built with various air-gaps. As a safety precaution, a bronze ring is placed next to the position sensor and acts as a second retainer bearing.

As part of the experiment, retainer bearings of various materials and ball bearings will be tested. Figure 6 shows the experimental set up and gives a survey on the measuring techniques.

Measurement Concepts

The aim of this experiment is to give a basis to the dynamical analysis that we have carried out and to verify its results. Figure 6 shows the measured variables and the instrumentation that has been installed.

The motion of the rotor is measured with four inductive sensors. When the rotor drops into the ball bearings, they are accelerated to the speed of the rotor in a few seconds. Two optical sensors measure the revolution of the ball-cage and the revolution of the inner ring of the bearing in order to quantify the sliding-rolling contact between the parts.

To quantify the energy loss and transport energy between the shaft and bearings, we will measure the temperature of the bearing and the spin of the rotor.

The contact forces are measured using two accelerometers.

Dell [7] showed that the impact load immediately following the failure must be the major design consideration. The shock is characterised by its maximum value F_0 and the duration of contact T_c (Figure 7), which is dependent on the properties of the rotor and the bearing.

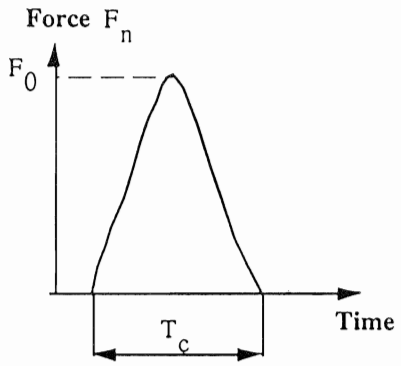

FIGURE 7: Impact Force

The purpose of this impact analysis is to determine the physical properties and to choose an appropriate measurement system to determine F_0 and T_c. Hertz impact theory [8] simplifies the analysis by assuming an impact to be quasi static.

From [8], we get the maximum force and the impact duration if a disk with mass m and radius r impacts the inside of a bearing with radius R. The speed of impact is V.

$$F_0 = 0.814\left[V^6 m^3 r E_r^2 (1 - (r/R))^{-1}\right]^{1/5} \quad (8)$$

$$T_c = 4.252\left[V^{-1}m^2r^{-1}E_r^{-2}(1-(r/R))\right]^{1/5} \quad (9)$$

E_r is the reduced modulus of elasticity of the rotor and the bearing. E_1 is the modulus of elasticity, and υ_1 the Poisson's ratio of the rotor, E_2, υ_2 of the bearing.

$$E_r = \left(\frac{1-\upsilon_1^2}{\pi E_1} + \frac{1-\upsilon_2^2}{\pi E_2}\right)^{-1} \quad (10)$$

Extensive numerical simulations for a steel rotor and a steel bearing have shown that the excitation frequency ($f_c = 1/T_c$) is higher than 3.5kHz.

In order to measure this contact force, we designed a force sensing device, with a natural frequency f_n higher than the excitation frequency f_c, thus avoiding amplification of the signal. It is suspended on special springs in order to separate the frequency ranges where measurements are of interest. The final version of the device is shown below.

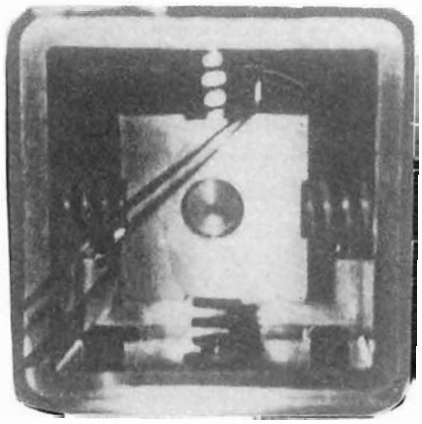

FIGURE 8. Force sensing device

Its two acceleration sensors are mounted on a plate and placed orthogonal to one another (one for each degree of freedom of the force sensing device). With this construction, we achieve a wide linear region between 500Hz and 8.4kHz. The peak at 500Hz is the rotational rigid mode of the construction, the peak at 8.4kHz is the first elastical mode of the mounting plate for the two accelerometers. The device was constructed in a away that it can be placed inside the experimental housing.

In order to measure the forces with accelerometers we must first calibrate our device. Figure 9 shows the transfer function of the device which was obtained from the response to a defined force impulse.

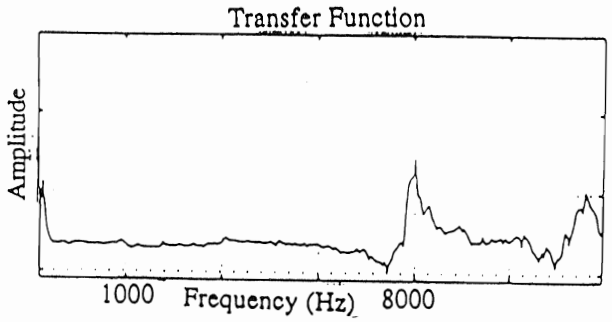

FIGURE 9. Transfer Function of the Force Measuring Device

During the experiment with our measurement platform the acceleration is measured in both directions. Dividing the Fourier transform of this measured acceleration by the obtained transfer function results in the force in the frequency domain. The inverse Fourier transform of this force results in the time domain solution.

Figure 10 shows a sample of impulse responses obtained from a sequence of contacts for a "prototype rotor" at 3000rpm. From the measured acceleration for one impulse the corresponding impulse force was derived.

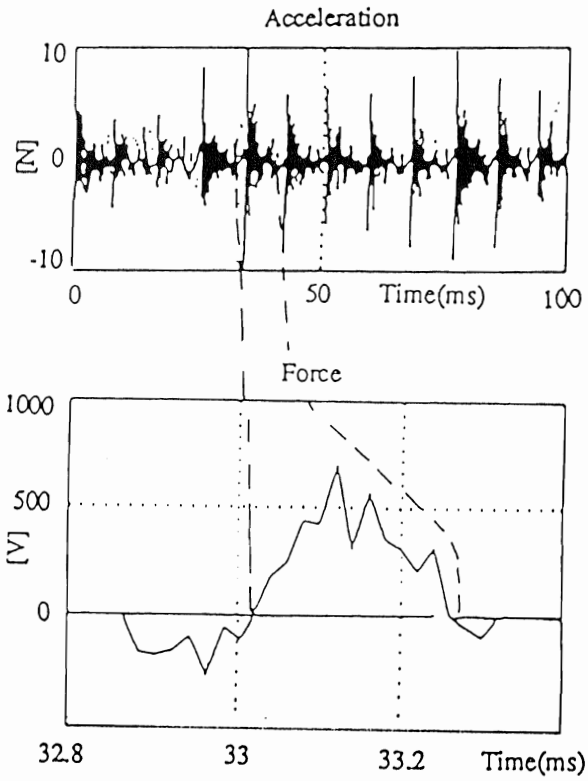

FIGURE 10. Measured Force

Within the interval 32.8ms and 33.4ms we receive a peak of acceleration and therefore of force. The contact time during the impact is 0.2ms, which corresponds to 5kHz. It shows that the excitation frequency f_c is inside the linear region of our force sensing device. This measurement was done with a sampling rate of 50kHz.

CONCLUSIONS

The effects of parameters on the impact dynamics have been analysed. The results show that in order to avoid the rotor whirl a retainer bearing should be designed with small friction, high damping and large air-gap. A force sensing device has been designed and measurement concepts have been presented.

REFERENCES

1. Diez, D., Entwurfs-Software für Mechatronik produkte mit Sicherheitsanforderungen - Beispiel Magnetlagersystem, Doct. Thesis ETH Nr. 10029, Zürich, 1993.
2. Ishi, T., Kirk, G.R., Transient Response Technique Applied to Active Magnetic Bearing Machinery During Rotor Drop, 13th Bienal Conf. on Mech. Vibration and Noise, ASME DE-Vol. 35, Rotating Machinery and Vehicle Dynamic, p. 191-199, 1991.
3. Schmied, M., Pradetto, B., Drop of Rigid Rotor in Retainer Bearings, Third Internat. Symp. on Magnetic Bearings, Washington, 1992.
4. Fumagalli, M., Feeny, B., Schweitzer, G., Dynamics of Rigid Rotor in Retainer Bearings, Third Internat. Symp. on Magnetic Bearings, Washington, 1992.
5. Szczygielski, W., and Schweitzer, G., Dynamics of High-Speed Rotor Touching a Boundary, IUTAM/ IFTOMM Symp. on Multibody Dynamics, CISM Udine, September 1985, Springer-Verlag, 1986.
6. Larsonneur, R., Design and Control of Active Magnetic Bearing Systems for High Speed Rotation, Doct. Thesis ETH Nr. 9140, Swiss Federal Institute of Technology, Zürich, 1992.
7. Dell, H., Engel, J., Faber, R., and Glass, D., Developments and Tests on Retainer Bearings for a Large Active Magnetic Bearings, First Internat. Symp. on Magnetic Bearings, ETH Zürich 1988, Springer-Verlag, 1988.
8. Engel, P. A., Impact Wear of Materials, Elsevier/ North-Holland Inc, 1976.